Journal of Luminescence 287 (2025) 121496

Contents lists available at ScienceDirect

Journal of Luminescence

journal homepage: www.elsevier.com/locate/jlumin

Detection of fluorescent low-energy proton tracks in lithium fluoride thin films on silicon substrates

Massimo Piccinini [a,*], Enrico Nichelatti [b], Valentina Nigro [a], Francesca Menchini [c], Marco Montecchi [c], Rosa Maria Montereali [a,1], Alessandro Ampollini [a], Concetta Ronsivalle [a], Maria Aurora Vincenti [a]

[a] ENEA C.R. Frascati, Nuclear Department, Via E. Fermi, 45, Frascati, 00044, Rome, Italy
[b] ENEA C.R. Casaccia, Nuclear Department, Via Anguillarese, 301, S. Maria di Galeria, 00123, Rome, Italy
[c] ENEA C.R. Casaccia, Energy Technologies Department, Via Anguillarese, 301, S. Maria di Galeria, 00123, Rome, Italy

ARTICLE INFO

Keywords:
Radiophotoluminescence
Color centers
Thin films
FNTD
Lithium fluoride
Proton beams

ABSTRACT

Recently, Fluorescent Nuclear Track Detectors (FNTDs) have been demonstrated in lithium fluoride (LiF) crystals exploiting the visible radiophotoluminescence (RPL) of F_2 and F_3^+ color centers (CCs). In this paper, solid-state radiation detectors based on LiF thin films, grown by thermal evaporation on Si(100) substrates, were tested as FNTDs with ~1 MeV proton beams produced by the vertical low-energy extraction line of the TOP-IMPLART linear accelerator in operation at ENEA Frascati. They were irradiated with the film surface approximately parallel to the beam propagation direction (i.e. the cleaved film edge was directly exposed to the incident beam). For the first time, at fluences between 10^7 and 10^8 protons/cm^2, luminescent images of single proton tracks were visualized in LiF films using a fluorescence microscope at high magnification. RPL spectra under continuous-wave blue laser excitation were also measured to study the behavior of the F_2 and F_3^+ emission bands, whose intensities show a different dependence on the excitation power. Increasing the proton beam fluence by two orders of magnitude, the superposition of a higher number of tracks allowed to fully detect the luminescent Bragg curve of the beam, even at this low proton energy. The energy spectrum of the proton beam was estimated by best fitting this luminescent Bragg curve, using FLUKA simulations of energy deposition in a LiF layer on Si. The layer was accurately modeled, and its density was derived from ellipsometric measurements of the refractive index.

1. Introduction

The use of passive radiation detectors enabling accurate measurements of integrated doses is necessary to ensure efficient and controlled utilization of ionizing radiation in numerous fields, including medical dosimetry, radiobiological research and industrial manufacturing [1]. Among them, Fluorescent Nuclear Track Detectors (FNTDs) are novel solid-state passive devices for single-particle detection based on the radiophotoluminescence (RPL) of stable electronic defects in insulating materials [2,3]. Due to the interaction with ionizing radiation, luminescent point defects are generated, whose local concentration depends on the energy deposited by the proton beam. Despite the lack of suitable materials [4,5], the RPL dosimetry technique has several advantages and can be used even to observe the track of a single ionizing particle, which loses energy along a certain distance as it travels through the material, provided that advanced fluorescence microscopy technologies with high spatial resolution are used. Proposed for the first time in doped crystalline Al_2O_3:C, Mg [6–8], initially applied to passive solid-state dosimetry of single charged particles and neutrons, other materials already used in dosimetry have shown promising performance when employed as FNTDs, such as Ag-activated alkali phosphate glasses [9–11] and nominally pure LiF crystals [12–14]. The systematic investigation of LiF crystals for the detection of luminescent proton tracks has been recently reported by our group at energies below 3 MeV [15,16] and also at much higher energies [17]. The visible RPL in LiF originates from the broad red and green emission bands of aggregate F_2 and F_3^+

This article is part of a special issue entitled: Scintillators & Dosimeters published in Journal of Luminescence.

* Corresponding author.
E-mail address: massimo.piccinini@enea.it (M. Piccinini).
[1] Current address: V. A. Cassani, 39, 00046 Grottaferrata (Rome), Italy.

https://doi.org/10.1016/j.jlumin.2025.121496
Received 27 June 2025; Received in revised form 6 August 2025; Accepted 24 August 2025
Available online 26 August 2025

color centers (CCs) [18], consisting of two and three electrons bound to two close anion vacancies, respectively, hosted in the face-centered cubic lattice of this alkali halide crystal. These laser-active defects [19], stable at room temperature, are simultaneously excited in their almost overlapping absorption bands, located at around 450 nm, known as a whole as the M band [20]. The wide tunability, combined with high gain coefficients, makes them attractive for the realization of miniaturized light-emitting photonic devices in LiF crystals [21] and thin films [22]. High-spatial resolution and well-contrasted X-ray images were also obtained in novel radiation imaging detectors based on RPL in LiF thin films [23,24] even at photon energies with attenuation lengths greater than the typical film thickness [25,26] and in extreme irradiation conditions [27], thanks to their compactness and easiness of use. With the growth of good optical quality LiF films on reflective substrates, such as silicon, the possibility to obtain radiation imaging detectors of enhanced sensitivity [28] was demonstrated [23,29]. Exploiting atomic-scale defects as minimum luminescent units, the thermal evaporation of LiF films on Ag-activated phosphate glass makes it possible to realize accurate X-ray two-dimensional (2D) dose-imaging detectors [30] with a wide dynamic range.

The use of radiation detectors based on RPL in LiF films has been successfully extended to proton beam advanced diagnostics [31], enabling 2D dose-mapping [32] and full Bragg curve acquisition [33]. The intensity of the visible RPL from the F_2 and F_3^+ defects in LiF films grows linearly with dose in a wide range of values for different types of radiation, including low-energy proton beams [34], and it is independent of the proton energy. An enhancement of the integrated RPL signal up to 50 % was obtained in optically transparent LiF films grown on a silicon substrate compared to those on glass [35]. In this paper, we report for the first time the imaging of luminescent low-energy proton tracks in optically transparent LiF thin films thermally evaporated on Si (100) substrates, along with a detailed investigation of the behavior of their visible RPL spectra as a function of the excitation laser power.

2. Materials and methods

At ENEA Frascati, optically transparent LiF films, about 1 μm thick, were grown by thermal evaporation on 0.5 mm thick Si(100) substrates, constantly kept at a temperature of 300 °C during deposition [36], which was performed in a vacuum chamber at a pressure below 1 mPa with a controlled deposition rate of 1 nm/s. The films were characterized by means of ellipsometric spectral measurements with a Woollam VASE instrument, and subsequently analyzed with the open-source software KSEMAW [37].

The films were cleaved into two halves and were then irradiated with the film surface approximately parallel to the beam propagation axis (edge-on irradiation). The cleaved film edge was directly exposed to the incident, nearly monochromatic, collimated pulsed proton beam delivered by the vertical extraction line of the TOP-IMPLART linear accelerator operating at ENEA Frascati [38]. The protons are produced by the PL7 injector, a commercial linac manufactured by ACCSYS-HITACHI, followed by a 90° dipole bending the beam into the vertical extraction line, which is 80 cm long and includes a 2 μm gold foil followed by a 2 mm diameter collimator. The gold foil is used to obtain a sufficiently homogeneous irradiation spot on the target. The protons are extracted in air through a 50 μm Kapton window with targets positioned 25 mm above it. The beam energy at the target can be tuned between 1 and 6 MeV, with fluence adjustable over several orders of magnitude. In this study, the proton beam energy was approximately 1 MeV, corresponding to a penetration range of ~13 μm in bulk LiF.

The proton track images were acquired using a Nikon Eclipse 80i fluorescence microscope, equipped with a Nikon TU Plan Fluor 100× objective (N.A. = 0.9) and a 440 nm pE-100 coolLED source for exciting the RPL of the CCs. The blue LED source intensity was set to illuminate the samples with a power density of ~0.7 W/cm^2 that we found to be a safe value in order to prevent photobleaching of the CCs. The RPL emission was filtered by a Chroma AT515lp filter and detected with an Andor NEO sCMOS camera operating at 16-bit, with 75 s acquisition time. The acquired images were processed using ImageJ software [39] and analyzed with the Monte Carlo software FLUKA, version 4–5.0 [40–42], in combination with its graphical user interface Flair, version 3.4–1 [43].

The RPL spectra of the irradiated LiF films were measured using an Andor iDus 401 CCD camera coupled to an Acton Research Spectra Pro 300i monochromator, under continuous-wave laser excitation at 445 nm.

3. Results and discussion

For the edge-on irradiation of the two halves of the LiF film on Si, two suitable fluence values were selected to ensure non-superimposed proton tracks. The pulsed beam from the accelerator was set at a charge of 0.5 pC/pulse, and 25 beam pulses were delivered to the first sample. The irradiation of a LiF crystal with its surface perpendicular to the beam propagation axis [15], allowed us to estimate a fluence of 5×10^7 protons/cm^2. Fig. 1 shows the fluorescence image of the proton tracks recorded at the edge of the half film irradiated under these conditions, along with an enlarged view of a region of interest (ROI) where individual tracks can be distinguished with a minimum lateral separation of ~1 μm.

The second sample was irradiated under the same conditions, but with 125 pulses delivered, resulting in an estimated fluence of 2.5×10^8 protons/cm^2. Fig. 2 shows the fluorescent proton tracks and the enlarged view of two ROIs. The first ROI, located close to the exposed edge of the film, shows a higher number of tracks than in Fig. 1, as expected due to the greater fluence; some track superpositions are observed, due also to slightly scattered proton trajectories, with a lateral separation $\ll 1$ μm among the tracks. The second ROI shows some fluorescent tracks of protons that did not directly enter the film through its edge, but rather through its surface due to a very small angular tilt of the sample. The tilt exposed the entire film surface directly to grazing-incidence protons, as sketched in the top-right picture of Fig. 3. By exploiting the enhancement of the visible RPL due to the presence of the reflecting Si substrate [35], along with the reduction of the background due to the limited physical thickness of the LiF film, it was possible to record entire proton tracks, approximately 15 μm in length, with a good signal-to-noise ratio.

To characterize the energy spectrum of the proton beam, another cleaved LiF film sample was irradiated by delivering 3750 pulses, corresponding to an estimated fluence of 1.9×10^{10} protons/cm^2. Under these conditions, the high proton fluence prevented the recording of individual tracks, because they resulted totally superimposed, as shown in the left picture of Fig. 3. By selecting a ROI in this image and integrating along the direction parallel to the film edge (x-axis), the luminescent Bragg curve of the beam protons was obtained. Indeed, the RPL intensity is proportional to the concentration of CCs [34], which in turn is proportional to the energy deposited by the proton beam along the penetration depth. The experimental Bragg curve was theoretically reproduced using the energy deposition profile of a proton beam in the LiF film as a function of penetration depth (z-axis), simulated with the Monte Carlo software FLUKA. The simulation also accounted for the presence of the Si substrate [33]. The beam energy parameters were manually adjusted to achieve optimal agreement with the experimental Bragg curve. Additionally, the film thickness and the LiF packing density were set to the values obtained from ellipsometric characterization, namely 1.18 μm and 88.6 %, respectively. The simulated proton beam, made of 10^8 virtual protons with a transverse size of 2.5×2.5 mm^2, was assumed to be collimated and vertically centered 250 μm below the interface between the Si substrate and the LiF film. The y-axis was defined as perpendicular to the film plane, with zero corresponding to the interface between the two materials (see the bottom-right picture in Fig. 3). To reproduce the experimental RPL curve also at depths beyond

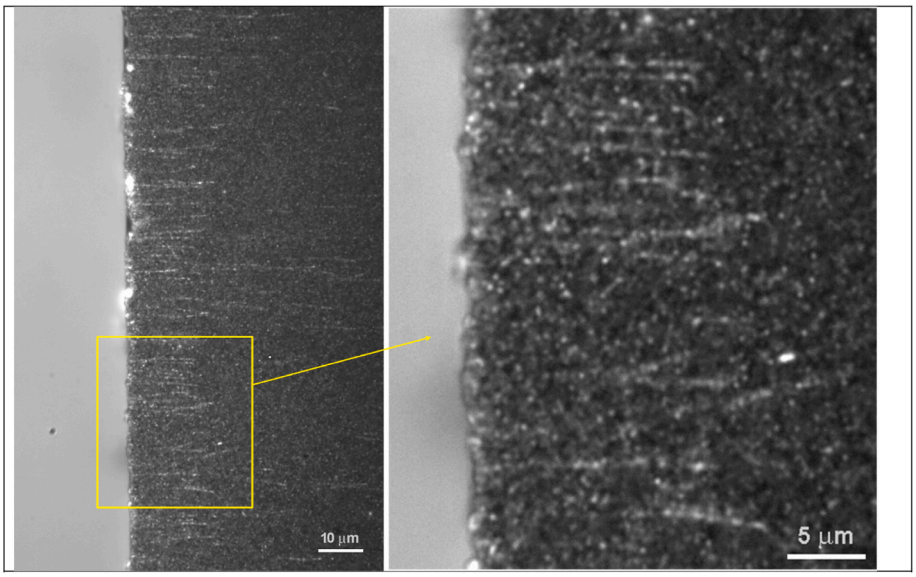

Fig. 1. *Left:* Fluorescence image of proton tracks recorded in a 1 μm-thick LiF film thermally evaporated on Si(100) and irradiated with a ~1 MeV beam impinging from the left on the cleaved film edge at a fluence of 5×10^7 protons/cm^2; *Right*: Enlarged view of the ROI.

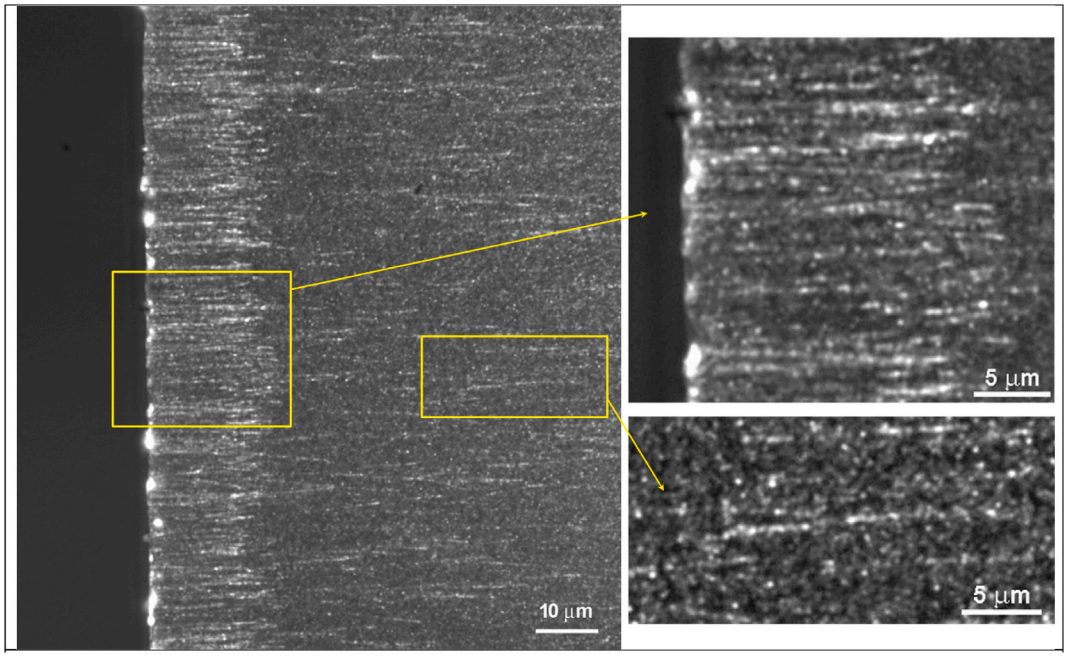

Fig. 2. *Left:* Fluorescence image of proton tracks recorded in a 1 μm-thick LiF film thermally evaporated on Si(100) and irradiated with a ~1 MeV beam impinging from the left on the cleaved film edge at a fluence of 2.5×10^8 protons/cm^2; *Right*: Enlarged view of two ROIs.

the Bragg peak, where the non-zero signal is attributed to sample tilting, the simulated beam was inclined downward by an angle of 0.85°, as if impinging from the half-space facing the film (see the top-right picture in Fig. 3). The comparison between the experimental RPL Bragg curve and the simulated one is reported in Fig. 4. The peak on the left side of the experimental Bragg curve is an artifact due to RPL scattering at the edge of the film, so it is used to set $z = 0$ in the graph, but it is not considered in the FLUKA simulation. Other parameters of the simulation were as follows: Gaussian proton energy spectrum with mean energy of 1.08 MeV and standard deviation of 82 keV; *Ekin Frac* parameter of the FLUKAFIX card set to 0.01 for both the LiF and Si materials; USRBIN scoring of deposited energy within the volume defined by -5 mm $\leq x \leq$ 5 mm (100 sampled points), -5 μm $\leq y \leq 3$ μm (400 sampled points), and -5 μm $\leq z \leq 30$ μm (350 sampled points).

The RPL intensity of the single proton tracks visualized by the fluorescence microscope is very low, so the blue LED excitation intensity was set at the maximum allowed power that prevented photobleaching of the CCs during image acquisition with the microscope. With the aim of studying the behavior of the F_2 and F_3^+ CCs emission bands with the excitation power, their RPL spectra under continuous-wave blue laser excitation were measured up to the highest available excitation powers comparable with those used in the microscope. To obtain RPL spectra of the CCs with a good signal-to-noise ratio, a 1.8 μm-thick LiF film, thermally evaporated on Si(100), was completely irradiated with the surface perpendicular to the proton beam direction under the same conditions at a dose of 8×10^3 Gy. The RPL spectra, measured by

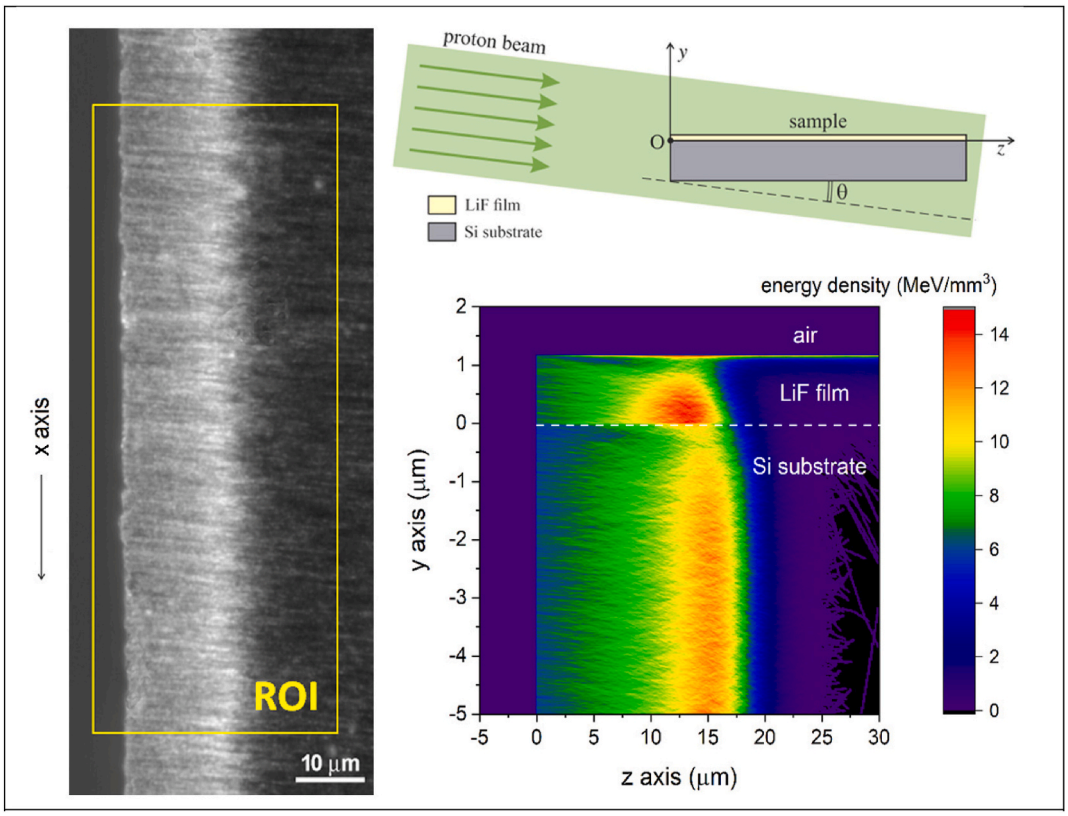

Fig. 3. *Left:* Fluorescence image of proton tracks recorded in a 1 μm-thick LiF film thermally evaporated on Si(100) and irradiated with a ~1 MeV beam impinging from the left on the cleaved film edge at a fluence of 1.9×10^{10} protons/cm^2; *Upper Right*: Scheme of the irradiation geometry; *Lower right*: Energy deposited by the proton beam in the LiF film and in the Si substrate as a function of proton penetration depth (z-axis), as simulated using FLUKA. The y-axis is perpendicular to the film plane and such that its zero corresponds to the interface between the LiF film and the Si substrate.

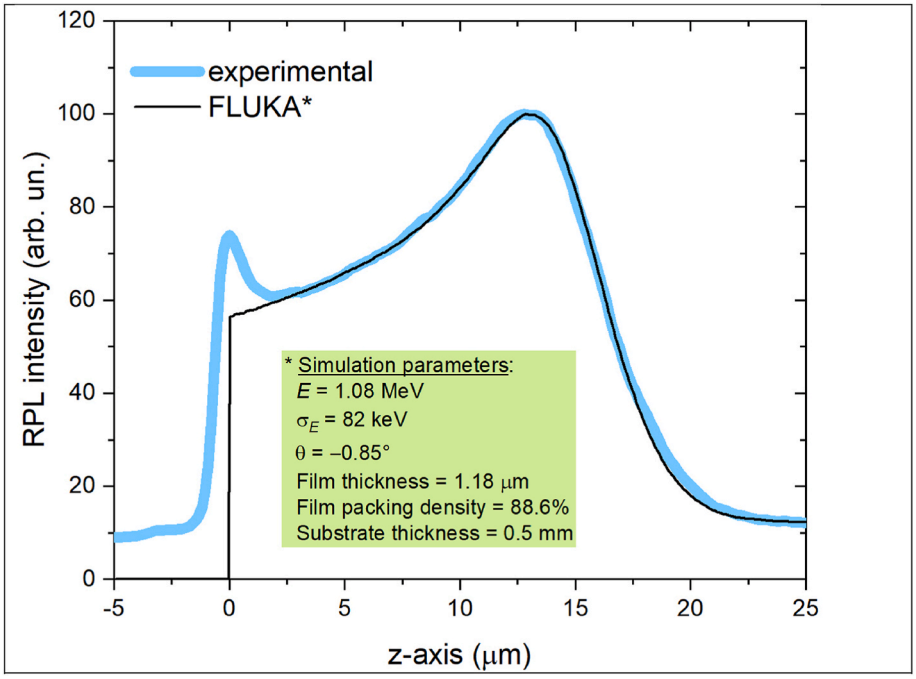

Fig. 4. Experimental RPL profile of the Bragg curve obtained by integrating along the x-axis the ROI of the left picture of Fig. 3 and its best-fitting curve obtained by FLUKA simulation.

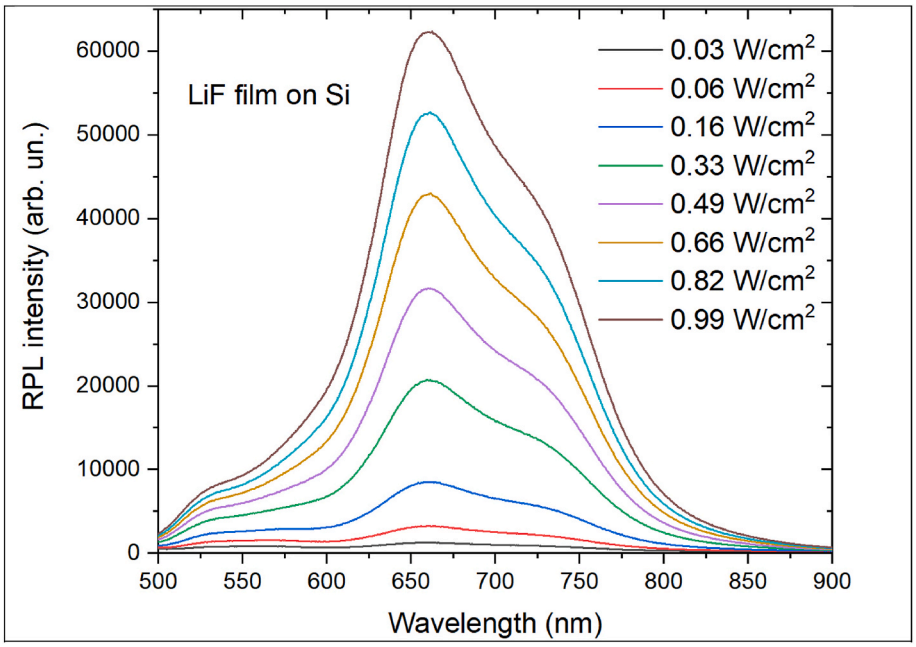

Fig. 5. RPL spectra of a 1.8 μm-thick LiF film thermally evaporated on Si(100), irradiated with a ~1 MeV proton beam at a dose of 8 × 10^3 Gy, measured at increasing power density of the CW laser excitation at 445 nm.

varying the excitation power density from 0.03 to 0.99 W/cm^2, are shown in Fig. 5. They consist of the superposition of the broad visible emission bands due to the F_2 and F_3^+ CCs, but are deformed due to the presence of the two material interfaces of the film: LiF-air and LiF-Si. Since one can assume that CCs emit radiation isotropically, part of the emitted RPL undergoes multiple reflections at these interfaces before reaching the detector. Each reflected component interferes, either destructively or constructively, with the others. The net effect depends on the wavelength, resulting in a distortion of the RPL spectra exiting the film and collected by the detector. To correct this deformation and obtain multireflection-free spectral distributions – as if the RPL were emitted by CCs embedded in a bulk LiF crystal – the energy spectrum exiting the film, resulting from a hypothetical flat spectral distribution within the film, was considered. This exiting spectrum was calculated using the theoretical model of light emission from a homogeneous volume source in an optical multilayer system [28]. The p-polarization state of the 445 nm excitation laser, its 23° angle of incidence with respect to the film normal, as well as the numerical aperture of the detection system (N.A. = 0.16) were properly taken into account in the calculation. The exiting spectrum calculated in this way can be considered the system response function to a flat spectral input. Therefore, the measured distorted spectra in Fig. 5 were corrected by dividing them, wavelength by wavelength, by this response function.

The corrected RPL spectra, shown in Fig. 6, were then analyzed by fitting the red and green F_2 and F_3^+ CCs emissions bands, respectively, with Gaussian functions of the photon energy for each power density value. Table 1 presents the parameters obtained from the multiband best fits of the RPL spectra. The reported parameters are: R^2, coefficient of determination; x_c, Gaussian center; σ, Gaussian standard deviation; A, Gaussian area. The uncertainties shown are evaluated at a 95 % confidence level. The areas under these Gaussian bands are plotted as functions of the excitation power density in Figs. 7 and 8, respectively. These figures also show the best fits obtained using the solutions of the four-level rate equations for the F_2 and F_3^+ CCs in LiF, assuming the presence of a triplet state for the F_3^+ centers [44,45]. For sufficiently low excitation levels, such that their ratios to the saturation intensity can be neglected, the solution for the F_2 centers is approximately linear with the excitation power density. On the other hand, due to the presence of a triplet state with a slow emptying rate, the solution for the F_3^+ centers

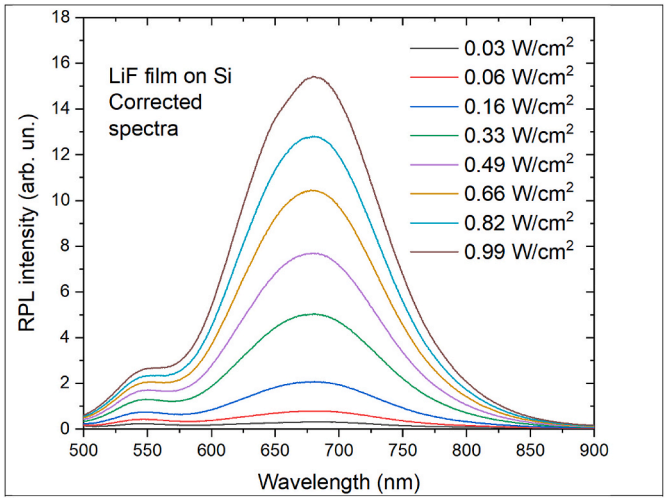

Fig. 6. Corrected RPL spectra (see text) of a 1.8 μm-thick thermally LiF film on Si(100), irradiated with a proton beam at a dose of 8 × 10^3 Gy, acquired at increasing power density of the CW laser excitation at 445 nm (see text for details).

exhibits a hyperbolic dependence on the excitation power density and cannot be linearized. Therefore, the function $AP/(1+BP)$ was utilized for fitting the F_3^+ data, where A and B are fitting parameters and P is the excitation power density. A comparison of the RPL band areas of F_2 and F_3^+ CCs, reported in Figs. 7 and 8, respectively, shows that at the highest excitation powers the F_3^+ emission band area is <5 % than that of the F_2 band. The blue LED excitation power density used in the fluorescence microscope for track image acquisition was ~0.7 W/cm^2, one of the highest ones used for the RPL spectra measurements. Consequently, the RPL signal observed in the fluorescent proton tracks images is primarily attributed to the F_2 CCs.

4. Conclusions

Optically transparent LiF thin films, thermally evaporated on Si(100)

Table 1
Gaussian multiband best fit parameters of the RPL spectra shown in Fig. 6.

Power density (W/cm^2)	R^2	F_2 band			F_3^+ band		
		x_c (eV)	σ (eV)	A (arb. un.)	x_c (eV)	σ (eV)	A (arb. un.)
0.03	0.951440	1.853 ± 0.002	0.206 ± 0.002	57.6 ± 0.8	2.295 ± 0.003	0.102 ± 0.003	5.4 ± 0.2
0.06	0.986873	1.841 ± 0.001	0.162 ± 0.001	120.5 ± 0.4	2.274 ± 0.002	0.114 ± 0.002	12.0 ± 0.2
0.16	0.997155	1.837 ± 0.001	0.149 ± 0.001	295.1 ± 0.8	2.264 ± 0.001	0.123 ± 0.001	22.3 ± 0.2
0.33	0.998882	1.836 ± 0.001	0.145 ± 0.001	700 ± 1	2.258 ± 0.001	0.131 ± 0.002	40.3 ± 0.4
0.49	0.998958	1.836 ± 0.001	0.144 ± 0.001	1068 ± 2	2.258 ± 0.001	0.129 ± 0.002	52.3 ± 0.8
0.66	0.999034	1.837 ± 0.001	0.144 ± 0.001	1447 ± 2	2.255 ± 0.002	0.131 ± 0.002	63.5 ± 0.7
0.82	0.998971	1.837 ± 0.001	0.144 ± 0.001	1775 ± 3	2.252 ± 0.002	0.132 ± 0.002	71 ± 1
0.99	0.998569	1.836 ± 0.001	0.144 ± 0.001	2135 ± 4	2.250 ± 0.002	0.132 ± 0.003	81 ± 1

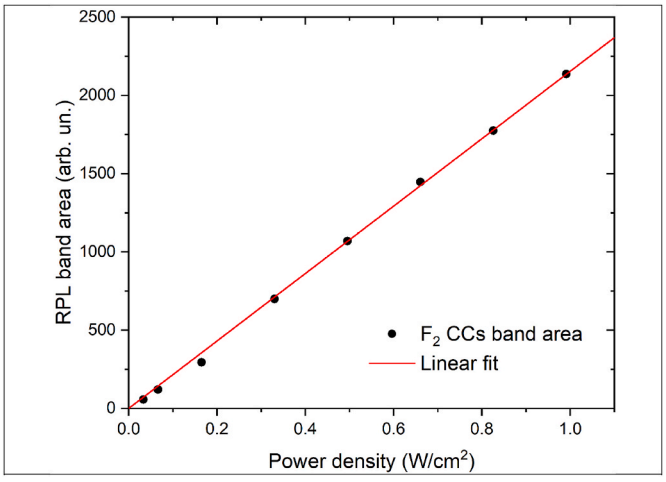

Fig. 7. F_2 CCs RPL Gaussian band area as a function of the laser power density, resulting from the spectra of Fig. 6, with its linear fit obtained using the solutions of the four-level rate equations.

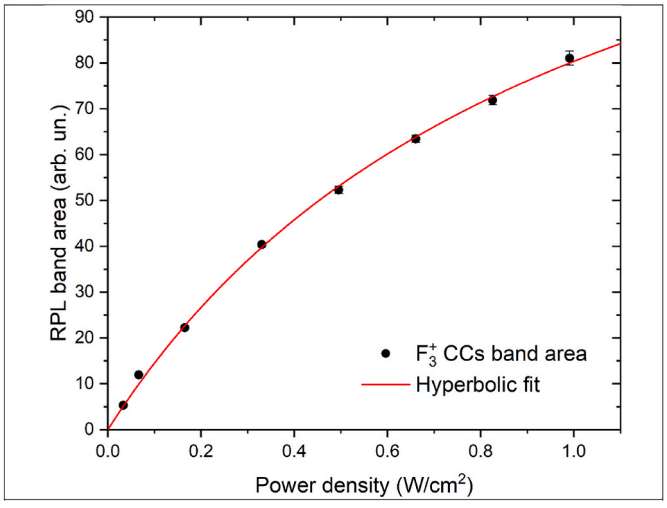

Fig. 8. F_3^+ CCs RPL Gaussian band area as a function of the laser power density, resulting from the spectra of Fig. 6, with its hyperbolic fit obtained using the solutions of the four-level rate equations and assuming the presence of a triplet state.

substrates, were successfully used, for the first time, as FNTDs for recording entire proton tracks of energy ~1 MeV at two fluence values between ~10^7 and ~10^8 protons/cm^2. Proton tracks are recorded in LiF films after irradiation due to the local formation of stable photoluminescent aggregate F_2 and F_3^+ CCs in the material lattice. Track images were successfully acquired using a fluorescence microscope at high magnification under blue LED excitation. This was possible thanks to the enhancement of the visible RPL, due to the reflecting Si substrate [35], and to the reduction of the background, due to the limited physical thickness of the LiF film, resulting in an improved signal-to-noise ratio. By increasing the beam fluence by two orders of magnitude, the superposition of a very high number of tracks in the RPL image enabled the extraction of the experimental Bragg curve. Its intensity profile was then successfully reproduced through FLUKA energy deposition simulations. These simulations, based on a layered LiF film model on a Si substrate with LiF density determined via ellipsometry, allowed the estimation of the beam average energy and energy spread. Since the RPL intensity of the track images is very low, a strong excitation power is needed to visualize the tracks at the fluorescence microscope with an acceptable signal-to-noise ratio. Therefore, the RPL intensities of the F_2 and F_3^+ CCs emission bands under laser excitation were studied as functions of the excitation power density up to levels comparable with those used at the microscope. After correcting the shape of the RPL spectra by considering the interference of the multiple RPL reflections at the LiF-air and LiF-Si interfaces of the film, the intensities of the F_2 and F_3^+ CCs bands showed different dependences on the excitation power. Due to the presence of a triplet excited state with a slow de-excitation rate in the four-level scheme of the F_3^+ CCs, approximately 95 % of the RPL signal of the tracks acquired at the fluorescence microscope was attributed solely to the red emission of F_2 CCs. These unique results highlight the potential of LiF thin films as FNTDs for the characterization of low-energy ion beams across various application fields.

CRediT authorship contribution statement

Massimo Piccinini: Writing – review & editing, Writing – original draft, Validation, Software, Methodology, Investigation, Formal analysis, Data curation, Conceptualization. **Enrico Nichelatti:** Writing – review & editing, Writing – original draft, Validation, Software, Methodology, Investigation, Formal analysis, Data curation, Conceptualization. **Valentina Nigro:** Writing – review & editing, Methodology, Conceptualization. **Francesca Menchini:** Writing – review & editing, Methodology, Conceptualization. **Marco Montecchi:** Writing – review & editing, Methodology, Conceptualization. **Rosa Maria Montereali:** Writing – review & editing, Writing – original draft, Resources, Project administration, Methodology, Investigation, Conceptualization. **Alessandro Ampollini:** Methodology, Investigation. **Concetta Ronsivalle:** Writing – review & editing, Methodology, Conceptualization. **Maria Aurora Vincenti:** Writing – review & editing, Supervision, Methodology, Conceptualization.

Declaration of competing interest

The authors declare that they have no known competing financial interests or personal relationships that could have appeared to influence the work reported in this paper.

Acknowledgements

Part of this work was carried out within the Project BIOTRACK, Fluorescent Nuclear Track Detectors for Radiobiology (2021–24), N. Prot. A0375-2020-36509, funded by Regione Lazio, L.R. 13/2008. The authors would like to thank E. Cisbani, C. De Angelis and G. Esposito for their valuable suggestions and discussions.

Data availability

Data will be made available on request.

References

[1] Z. Yang, H. Vrielinck, L.G. Jacobsohn, P.F. Smet, D. Poelman, Passive dosimeters for radiation dosimetry: materials, mechanisms, and applications, Adv. Funct. Mater. (2024) 2406186.
[2] J.H. Schulman, W.D. Compton, Color Centers in Solids, Pergamon Press, Oxford, UK, 1963.
[3] S.W.S. McKeever, A Course in Luminescence Measurements and Analyses for Radiation Dosimetry, Wiley, 2022.
[4] T. Yanagida, G. Okada, T. Kato, D. Nakauchi, N. Kawaguchi, A review and future of RPL dosimetry, Radiat. Meas. 158 (2022) 106847.
[5] G. Okada, Y. Koguchi, T. Yanagida, S. Kasap, H. Nanto, Recent advances in radiation-induced luminescence materials, Jpn. J. Appl. Phys. 62 (2023) 010609.
[6] G.M. Akselrod, M.S. Akselrod, E.R. Benton, N. Yasuda, *A novel Al_2O_3 fluorescent nuclear track detector for heavy charged particles and neutrons*, Nucl. Instrum. Methods B 247 (2006) 295.
[7] M.S. Akselrod, G.J. Sykora, Fluorescent nuclear track detector technology—a new way to do passive solid state dosimetry, Radiat. Meas. 46 (2011) 1671.
[8] M. Akselrod, J. Kouwenberg, Fluorescent nuclear track detectors – review of past, present and future of the technology, Radiat. Meas. 117 (2018) 35.
[9] T. Kurobori, Y. Yanagida, S. Kodaira, T. Shirao, Fluorescent nuclear track images of Ag-activated phosphate glass irradiated with photons and heavy charged particles, Nucl. Instrum. Methods A 855 (2017) 25.
[10] S. Kodaira, T. Kusumoto, H. Kitamura, Y. Yanagida, Y. Koguchi, *Characteristics of fluorescent nuclear track detection with Ag^+-activated phosphate glass*, Radiat. Meas. 132 (2020) 106252.
[11] T. Yamamoto, D. Maki, F. Sato, Y. Miyamoto, H. Nanto, T. Iida, The recent investigations of radiophotoluminescence and its application, Radiat. Meas. 46 (12) (2011) 1554.
[12] P. Bilski, B. Marczewska, Fluorescent detection of single tracks of alpha particles using lithium fluoride crystals, Nucl. Instrum. Methods B 392 (2017) 41.
[13] P. Bilski, B. Marczewska, M. Kłosowski, W. Gieszczyk, M. Naruszewicz, Detection of neutrons with LiF fluorescent nuclear track detectors, Radiat. Meas. 116 (2018) 35.
[14] P. Bilski, B. Marczewska, W. Gieszczyk, M. Kłosowski, M. Naruszewicz, Y. Zhydachevskyy, M. Sankowska, S. Kodaira, Fluorescent imaging of heavy charged particle tracks with LiF single crystals, J. Lumin. 213 (2019) 82.
[15] M. Piccinini, E. Nichelatti, G. Esposito, E. Cisbani, V. Nigro, M.A. Vincenti, F. Limosani, C. Ronsivalle, A. Ampollini, C. De Angelis, R.M. Montereali, Detection of fluorescent low-energy proton tracks in lithium fluoride crystals, Radiat. Meas. 174 (2024) 206701.
[16] E. Nichelatti, M. Piccinini, A. Ampollini, P. Anello, M.D. Astorino, G. Bazzano, E. Cisbani, C. De Angelis, G. Esposito, F. Limosani, P. Nenzi, V. Nigro, C. Ronsivalle, F. Santavenere, V. Surrenti, E. Trinca, M.A. Vincenti, R. M. Montereali, Energy spectrum of protons below 10 MeV using color-center radiophotoluminescence in LiF crystals: a Monte Carlo-supported random-optimization estimator, Nucl. Instrum. Methods A 1072 (2025) 170218.
[17] P. Bilski, B. Marczewska, M. Sankowska, A. Kilian, J. Swakoń, Z. Siketić, P. Olko, Detection of proton tracks with LiF fluorescent nuclear track detectors, Radiat. Meas. 173 (2024) 107083.
[18] G. Baldacchini, E. De Nicola, R.M. Montereali, A. Scacco, V. Kalinov, Optical Bands of F_2 and F_3^+ centers in LiF, J. Phys. Chem. Solid. 61 (2000) 21.
[19] T.T. Basiev, S.B. Mirov, V.V. Osiko, Room-temperature color center lasers, IEEE J. Quant. Electron. 24 (1988) 1052.
[20] J. Nahum, D.A. Wiegand, Optical properties of some F -Aggregate centers in LiF, Phys. Rev. 154 (1967) 817.
[21] R.M. Montereali, V. Mussi, E. Nichelatti, M. Piccinini, Photonics in wide-band-gap materials: the challenge of color-center waveguides in lithium fluoride, Opt. Mater. 160 (2025) 116719.
[22] R.M. Montereali, Green-red photoluminescence from colored LiF films for integrated active devices, J. Lumin. 72–74 (1997) 4.
[23] G. Baldacchini, F. Bonfigli, A. Faenov, F. Flora, R.M. Montereali, A. Pace, T. Pikuz, L. Reale, Lithium fluoride as a novel X-Ray image detector for biological μ-World capture, J. Nanosci. Nanotechnol. 3 (6) (2003) 483.
[24] R.M. Montereali, F. Bonfigli, M. Piccinini, E. Nichelatti, M.A. Vincenti, Photoluminescence of colour centres in lithium fluoride thin films: from solid-state miniaturised light sources to novel radiation imaging detectors, J. Lumin. 170 (2016) 761.
[25] S. Almaviva, F. Bonfigli, I. Franzini, A. Lai, R.M. Montereali, D. Pelliccia, A. Cedola, S. Lagomarsino, Hard X-Ray contact microscopy with 250 nm spatial resolution using a LiF film detector and a tabletop microsource, Appl. Phys. Lett. 89 (2006) 54102.
[26] F. Bonfigli, A. Cecilia, S. Heidari Bateni, E. Nichelatti, D. Pelliccia, F. Somma, P. Vagovic, M.A. Vincenti, T. Baumbach, R.M. Montereali, In-line X-ray lensless imaging with lithium fluoride film detectors, Radiat. Meas. 56 (2013) 277.
[27] T.A. Pikuz, A. Ya Faenov, Y. Fukuda, M. Kando, P. Bolton, A. Mitrofanov, A. V. Vinogradov, M. Nagasono, H. Ohashi, M. Yabashi, K. Tono, Y. Senba, T. Togashi, T. Ishikawa, Soft x-ray free-electron laser imaging by LiF crystal and film detectors over a wide range of fluences, Appl. Opt. 52 (2013) 109.
[28] E. Nichelatti, R.M. Montereali, Photoluminescence from a homogeneous volume source within an optical multilayer: analytical formulas, J. Opt. Soc. Am. A 29 (3) (2012) 303.
[29] M.A. Vincenti, E. Nichelatti, V. Nigro, M. Piccinini, B. Albertazzi, Y. Benkadoum, H. Dabrowski, M. Koenig, G. Rigon, P. Mabey, P. Mercere, P. Da Silva, T. Pikuz, N. Ozaki, E. Filippov, S. Makarov, S. Pikuz, R.M. Montereali, Visible radiophotoluminescence of color centers in lithium fluoride thin films for high spatial resolution imaging detectors for hard X-rays, ECS J. Solid State Sci. Technol. 12 (2023) 066008.
[30] T. Kurobori, A. Matoba, Development of accurate two-dimensional dose-imaging detectors using atomic-scale color centers in Ag-activated phosphate glass and LiF thin films, Jpn. J. Appl. Phys. 53 (2014) 02BD14.
[31] M. Piccinini, F. Ambrosini, A. Ampollini, M. Carpanese, L. Picardi, C. Ronsivalle, F. Bonfigli, S. Libera, M.A. Vincenti, R.M. Montereali, Solid state detectors based on point defects in lithium fluoride for advanced proton beam diagnostics, J. Lumin. 156 (2014) 170.
[32] M. Piccinini, E. Nichelatti, A. Ampollini, L. Picardi, C. Ronsivalle, F. Bonfigli, S. Libera, M.A. Vincenti, R.M. Montereali, Proton beam dose-mapping via color centers in LiF thin film detectors by fluorescence microscopy, EPL 117 (2017) 37004.
[33] R.M. Montereali, V. Nigro, M. Piccinini, M.A. Vincenti, A. Ampollini, P. Nenzi, C. Ronsivalle, E. Nichelatti, Bragg curve detection of low-energy protons by radiophotoluminescence imaging in lithium fluoride thin films, Sensors 23 (2023) 4779.
[34] M. Piccinini, F. Ambrosini, A. Ampollini, L. Picardi, C. Ronsivalle, F. Bonfigli, S. Libera, E. Nichelatti, M.A. Vincenti, R.M. Montereali, Photoluminescence of radiation-induced color centers in lithium fluoride thin films for advanced diagnostics of proton beams, Appl. Phys. Lett. 106 (2015) 261108.
[35] M.A. Vincenti, M. Leoncini, S. Libera, A. Ampollini, A. Mancini, E. Nichelatti, V. Nigro, L. Picardi, M. Piccinini, C. Ronsivalle, A. Rufoloni, R.M. Montereali, Enhanced F_2 and F_3^+ colour centres photoluminescence response of LiF film-based detectors for proton beams, Opt. Mater. 119 (2021) 111376.
[36] M. Leoncini, M.A. Vincenti, F. Bonfigli, S. Libera, E. Nichelatti, M. Piccinini, A. Ampollini, L. Picardi, C. Ronsivalle, A. Mancini, A. Rufoloni, R.M. Montereali, Optical investigation of radiation-induced color centers in lithium fluoride thin films for low-energy proton-beam detectors, Opt. Mater. 88 (2019) 580.
[37] M. Montecchi, A. Mittiga, C. Malerba, F. Menchini, KSEMAW: an open source software for the analysis of spectrophotometric, ellipsometric and photothermal deflection spectroscopy measurement, Open Res. Eur. 1 (2023) 95, https://doi.org/10.12688/openreseurope.13842.2.
[38] L. Picardi, A. Ampollini, G. Bazzano, E. Cisbani, F. Ghio, R.M. Montereali, P. Nenzi, M. Piccinini, C. Ronsivalle, F. Santavenere, V. Surrenti, E. Trinca, M. Vadrucci, E. Wembe Tafo, Beam commissioning of the 35 MeV section in an intensity modulated proton linear accelerator for proton therapy, Phys. Rev. Accel. Beams 23 (2020) 020102.
[39] ImageJ (*image processing and analysis in java*), Available online: https://imagej.net/ij/index.html.
[40] Website. https://fluka.cern.
[41] G. Battistoni, T. Boehlen, F. Cerutti, P.W. Chin, L.S. Esposito, A. Fassò, A. Ferrari, A. Lechner, A. Empl, A. Mairani, A. Mereghetti, P. Garcia Ortega, J. Ranft, S. Roesler, P.R. Sala, V. Vlachoudis, G. Smirnov, Overview of the FLUKA code, Ann. Nucl. Energy 82 (2015) 10.
[42] C. Ahdida, D. Bozzato, D. Calzolari, F. Cerutti, N. Charitonidis, A. Cimmino, A. Coronetti, G.L. D'Alessandro, A. Donadon Servelle, L.S. Esposito, R. Froeschl, R. García Alía, A. Gerbershagen, S. Gilardoni, D. Horváth, G. Hugo, A. Infantino, V. Kouskoura, A. Lechner, B. Lefebvre, G. Lerner, M. Magistris, A. Manousos, G. Moryc, F. Ogallar Ruiz, F. Pozzi, D. Prelipcean, S. Roesler, R. Rossi, M. Sabaté Gilarte, F. Salvat Pujol, P. Schoofs, V. Stránský, C. Theis, A. Tsinganis, R. Versaci, V. Vlachoudis, A. Waets, M. Widorski, New capabilities of the FLUKA multi-purpose code, Front. Phys. 9 (2022) 788523.
[43] A. Donadon, G. Hugo, C. Theis, V. Vlachoudis, FLAIR3 – recasting simulation experiences with the advanced interface for FLUKA and other Monte Carlo codes, EPJ Web Conf. 302 (2024). SNA + MC 2024).
[44] G. Baldacchini, M. Cremona, G. d'Auria, R.M. Montereali, V. Kalinov, Radiative and nonradiative processes in the optical cycle of the F_3^+ center in LiF, Phys. Rev. B 54 (1996) 17508.
[45] E. Nichelatti, M. Piccinini, M. Pimpinella, V. De Coste, R.M. Montereali, Spectral analysis of visible photoluminescence from F_2 and F_3^+ color centers in low-dose gamma-irradiated lithium fluoride crystals at increasing excitation power, J. Lumin. 241 (2022) 118483.